Cellulose (2016) 23:545–555
DOI 10.1007/s10570-015-0844-3

ORIGINAL PAPER

Incorporation of *Aloe vera* extracts into nanocellulose during biosynthesis

Joanna F. Godinho · Fernanda V. Berti · Daliana Müller · Carlos R. Rambo · Luismar M. Porto

Received: 13 February 2015 / Accepted: 9 December 2015 / Published online: 22 December 2015

Abstract Bacterial nanocellulose (BC) and *Aloe vera* composites were synthesized in situ by *Gluconacetobacter hansenii* using mannitol-based medium supplemented with 60 % (v/v) of three different *Aloe vera* portions (*Aloe vera* gel pulp, *Aloe vera* gel extract and polysaccharide fraction) under static conditions. The chemical interactions, morphology, crystallinity and mechanical properties influenced by aloe supplementation into BC medium were characterized. The interactions between BC and *Aloe*, characterized by X-ray photoelectron spectroscopy and Fourier transform infrared spectroscopy, revealed the presence of nitrogenous compounds and aliphatic chains into BC–*Aloe* composites (BCAC). Moreover, *Aloe* portions reduced the crystallinity and crystallite size of BCAC, as shown by X-ray diffractometry. The *Aloe vera* compounds deposited onto BC fibers disrupted the hydroxyl interactions, decreasing the Young's modulus as well as the tensile strength and water uptake of BCAC. However, aloe incorporation of aloe fractions promoted an increase of the extensibility of BCAC (elongation at break), allowing fiber movement. Live/Dead® cell viability assays revealed a strong adhesion between L929 cells and the surface of BC and BCAC. The results indicated that this material could be successfully applied as a biomaterial for several biomedical applications, a scaffold for skin substitution and regeneration, and cell culture substrates.

Keywords *Aloe vera* · Bacterial nanocellulose · Nanocomposites · Polysaccharides

J. F. Godinho · F. V. Berti · L. M. Porto
Department of Chemical and Food Engineering, Federal University of Santa Catarina, Florianópolis, SC 88040-900, Brazil

D. Müller
Department of Mechanical Engineering, Federal University of Santa Catarina, Florianópolis, SC 88040-900, Brazil

C. R. Rambo (✉)
Department of Electrical and Electronic Engineering, Federal University of Santa Catarina, Florianópolis, SC 88040-900, Brazil
e-mail: carlos.rambo@ufsc.br

Introduction

Cellulose is the main component of vegetal biomass and most biodegradable material available in nature, also being synthesized by a few bacteria of the genus *Gluconacetobacter*. Bacterial cellulose (BC) is extracellularly secreted in the form of nanofibers, randomly distributed, which are interconnected and form a highly entangled three-dimensional structure with a unique porous matrix, mechanical properties, and high water absorption, surface area and crystallinity (Chang and Zhang 2011; Klemm et al. 2005). Moreover, the physical, structural and mechanical properties of BC

can be enhanced using alternative substrates or blending compounds during BC synthesis or post-synthesis to produce materials suitable as scaffolds for biomedical applications (Czaja et al. 2007; Müller et al. 2012). Recent studies have reported the modification of chemical and physical properties of BC through incorporation of active substances in the culture medium (Stumpf et al. 2013; Berti et al. 2013).

Aloe vera (*Aloe barbadensis* Miller) is a perennial succulent, originated from South Africa, belonging to the Asphodelaceae family (Grace et al. 2008). The mucilaginous inner gel of *Aloe vera* is composed of over 25 % polysaccharides (dry matter) and has the greatest range of biological activities, such as antiinflammatory, immunomodulating, antibacterial as well as accelerating healing processes, reported in the literature (Reynolds 2004; Grindlay and Reynolds 1986. Zhang and Tizard 1996). The main constituents of the polysaccharide fraction of *Aloe vera* L. are mannose (around 94 %), glucose (∼4 %) and uronic acid (∼2 %). Traces of rhamnose and arabinose can also be found (Campestrini et al. 2013). Furthermore, the complex mix of proteins, carbohydrates, saccharides, vitamins, inorganic and organic compounds of *Aloe vera* extract has been reported to have a synergetic effect and offers an alternative therapy to treat health disorders such as constipation, diabetes and wound healing (Reynolds 2004; Kim et al. 2009). Due to the biological activity, *Aloe vera* has been blended to chitosan and alginate in the development of new classes of materials with optimized properties for biomedical applications (Silva et al. 2013a; Pereira et al. 2013).

Recently, Saibuatong and Phisalaphong (2010) reported the production of an *Aloe vera*–BC composite. They explored the incorporation of the *Aloe vera* gel into BC during biosynthesis. However, since *Aloe vera* gel comprises a mixture of different compounds whose wt % fractions may vary depending on several factors, the influence of each one separately on the microstructure and mechanical properties is still not well understood. This work reports on the supplementation of mannitol-based medium for nanocellulose biosynthesis enriched with different *Aloe vera* extract fractions to produce BC–*Aloe* composites (BCACs). The effect of each different extract on the morphology, water uptake, mechanical properties, crystallinity, biocompatibility and chemical composition of BCACs was evaluated and compared to that on pure BC membranes.

Materials and methods

Extraction of the *Aloe vera* gel pulp (GP), *Aloe vera* gel extract (GE) and polysaccharide fraction (PF).

Fifteen leaves of *Aloe barbadensis Miller* were obtained from *Naturama Sucos Integrais do Brasil* (Paulo Lopes, SC, Brazil). In a first step the leaves were cleaned with water and immersed in a calcium hypochlorite solution (0.125 g/l) for 5 min, and then the excess was removed with distilled water. The leaves were separated into three groups with five leaves each. After removing the peel, the leaf pulp was milled; one portion was separated and identified as *Aloe vera* gel pulp (GP). This portion was mainly composed of aloe inner gel and pulp fibers. The *Aloe vera* gel extract (GE) was obtained by centrifugation at $3335\times g$ for 15 min at 25 °C. Submitting GE to alcoholic precipitation with 6:1 volumes of ethanol for 24 h at room temperature resulted in a white supernatant, which was collected, centrifuged at $3335\times g$ for 15 min at 25 °C, separated from the ethanol, immersed in distilled water and autoclaved. The resulting solution was lyophilized, and the white powder was denoted the *Aloe vera* polysaccharide fraction (PF). An aqueous solution of 1 g/l of the polysaccharide fraction was prepared for composite production.

Bacterial strain and cellulose production

The *Gluconacetobacter hansenii* strain, ATCC 23769, from the "Collection of Tropical Culture (CCT)" (André Tosello Foundation, Brazil) was used in this work.

The medium culture was prepared with mannitol (25 g), bactopeptone (3.0 g) and yeast extract (5.0 g) in 1 l of distilled water, adjusted to pH 6.6 and sterilized. To produce the modified BC–*Aloe* composites, a specific bacterial culture medium was produced through the addition of 60 % (v/v) of each portion (PF, GE and GP). The usual bacterial culture medium without *Aloe* was used to produce the BC control. Subsequently, 10 % of the precultured bacterium was added to each bacterial medium culture. A 24-well

plate was used to synthesize BC–*Aloe* membranes, with 1 ml in each well, for 10 days under static conditions at room temperature (25 °C). For purification, the BC–Aloe scaffolds were submitted to a treatment with 0.1 M of NaOH solution for 24 h at 50 °C and then washed with distilled water. The pH was adjusted to 7 and sterilized by autoclaving (120 °C for 20 min) before storage. The BC–*Aloe* scaffolds formed were identified as BC-60PF, BC-60GE and BC-60GP.

Characterization of BC and BCAC

To determine the water uptake, the dried BCACs were weighed (W_d) and then immersed in distilled water for 24 h to achieve a swollen state. Then the water excess on the surface was removed with paper, and the wet BCAC membranes were weighted (W_w). The water uptake was then determined by the relation: $W_u = (W_w - W_d)/W_d$, where an average of the triplicate value was considered.

The BC and BCAC in the hydrogel and freeze-dried state were submitted to tensile tests on a TA-XTplus texturometer (Stable Micro Systems Texture Analyzer) using a 500-N load cell at room temperature and humidity conditions, operating at a deformation rate of 0.5 mm/s. The sample dimensions were 92 × 14 × individual sample thickness (mm). Young's modulus (E), tensile strength (σ) and elongation at break (ε_b) were determined from the stress/strain curve using Exponent 5.1.1 software. Three specimens were analyzed for each sample type.

The freeze-dried samples were analyzed by Fourier transformed infrared spectroscopy performed in a Bruker instrument, model TENSOR 27, with an ATR accessory and ZnSe crystal. Spectra of BCAC were recorded at a 4000–600 cm^{-1} range with a 4 cm^{-1} resolution and accumulation of 16 scans.

The microstructure of the samples was evaluated through scanning electron spectroscopy (SEM, JEOL JSM-6390LV) operating at 10 kV. SEM images were further analyzed (ImageJ®) to estimate the porosity, fiber size and surface fiber density of the BC and BCAC. For SEM analysis the materials were frozen (at −80 °C) and lyophilized for 24 h. For cross-section analysis, samples were first frozen in nitrogen liquid (2 min) and then cut. The samples were then placed on an aluminum support and finally sputtered with gold.

XRD diffraction spectra of freeze-dried samples were collected on a Philips diffractometer (model X'Pert) with CuKα radiation ($\lambda = 0.154$ nm). Measurements were made over a 2θ interval of 5° to 40° with 1°/min steps. The crystallinity index (χ_c) of BC films was estimated from the ratio between the areas under the main crystalline peaks and the total area of the diffractogram as described by Watanabe et al. (1998). The crystallite size was estimated by Scherrer's equation at the (200) peak as described by Nieduszy and Preston (1970) and Tokoh et al. (1998).

X-ray photoelectron spectroscopy analysis of BCAC was performed using a VSW HA-100 spherical analyzer equipped with an Al (Kα) X-ray source operating at 15 kV, and the spectrometer was calibrated using Ag 3d5/2 as reference. Data were collected at a pressure below 1×10^{-6} Pa. The spectra were obtained with 50-eV constant pass energy, and high-resolution spectra were taken at a pass energy of 20 and 0.1 eV of the energy step. Spectral analysis was performed using peak fitting with the Gaussian peak shape and linear background subtraction. The binding energy scale was referred to the oxygen in the O1s spectra at 532.9 eV.

All data were statically evaluated via Statics 7.0 (StatSoft Software, Tulsa, OK, USA) by one-way analysis of variance (ANOVA) and Tukey's test in which $p < 0.05$ was considered statistically significant. The results were expressed as the mean ± standard error.

Cell culture and viability assay

An established mouse fibroblast cell line (L929), cultured in DMEM high glucose (Life Technologies, USA) supplemented with 10 % fetal bovine serum and 1 % penicillin/streptomycin, was used to assess the viability of cells cultured on BC–*Aloe* and BC samples. L929 cells were maintained at 37 °C in an incubator containing 5 % CO_2 and 95 % humidified air during the in vitro tests.

The fluorescence-based Live/Dead® (Life Technologies Corp., USA) assay was used to analyze the cell viability of L929 cultured on BC–*Aloe* and BC samples. Before the cell seeding, the sterilized BC–*Aloe* and BC samples were placed in the bottom of 24-well culture plates (TPP Techno Plastic Products, Switzerland). After that, 500 µl of incomplete (without fetal bovine serum) DMEM medium was added over each sample to perform the exchange of PBS to DMEM. The samples were kept with incomplete

culture medium for 24 h at 37 °C. Following this, the incomplete medium was removed, and 10^5 cells/sample were seeded on top of the entangled surfaces of BC–*Aloe* and BC samples. After 48 h, the culture medium (DMEM) was removed and the samples washed three times with PBS. Subsequently, 100 µl of sterile PBS solution containing 1:4 of calcein and ethidium homodimer-1 was added over each sample. Samples were incubated into calcein/ethidium homodimer solution for 20 min at 37 °C. A fluorescence microscope (Nikon EclipseCi-L, Tokyo, Japan) was used to analyze the cell viability of L929 cultured on BC–*Aloe* and BC samples. Viable cells were quantified using image analysis (ImageJ®) (Shaik et al. 2013). For analysis, three regions of three Live-Dead images of each sample were randomly selected.

Results and discussion

Figure 1 shows the water uptake of BC samples. As shown, BC was capable of absorbing an average of 89 g of water per gram of dried cellulose. BC-60PF presented a decrease of 25 % compared to the control. A slight decrease of adsorbed water was obtained for BC-60GE and BC-60GP compared to pure BC. Despite this slight decrease, the capability to absorb water is still under those observed for BC. Water uptake is intimately linked to the microstructure characteristics produced by the insertion of PF, GE or GP in the membranes. Several factors can change the absorption behavior, such as variations in the composition of the culture medium, which involves

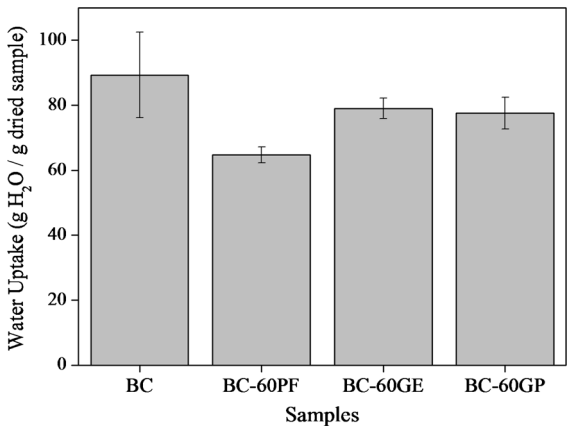

Fig. 1 Water uptake of BC, BC-60PF, BC-60GE and BC-60GP

the carbon sources that can affect the fermentation time as well as the post-treatment and drying process (Tang et al. 2010; Guo and Catchmark 2012). The reduction of water uptake in BC-60PF composites is in accordance with the values reported in the literature. It was reported that a reduction of water uptake could be influenced by crosslinking between chitosan and *Aloe vera*, even when the aloe concentrations were lower than 30 % (v/v), which occurred by decreasing the content of the available $–NH_2–$ groups, which are capable of forming hydrogen interactions with water (Silva et al. 2013a, b; Pereira et al. 2010; Jithendra et al. 2013). Crosslinking between BC and plant cell wall polysaccharides occurs as a result of the enthalpic driving force, and once microfibrils are available, the polysaccharide interacts by crosslinkage to another microfibril, reducing the availability of hydroxyl groups from BC to make hydrogen bonds with water. On the other hand, the addition and availability of hydrophilic groups from *Aloe vera* on the material's surface could explain the comparable water uptake of BC-60GE and BC-60GP with pure BC.

The microstructures of the upper, bottom and inner surface (cross-section) of BC and BCAC are shown in the SEM micrographs in Fig. 2. The typical structure of a dense network on an air/medium interface connected by a porous network with pores of varying sizes extending to the porous underside of BC was observed (Fig. 2a–c). In the presence of GE and GP, the upper surface remains highly closed (Fig. 2g, j), but when PF was added, some porous regions were observed on the upper surface (Fig. 2d). The bottom surface of BC-60PF and BC-60GE samples revealed some entrapped polysaccharides between the CB fibers (Fig. 2e and h), respectively. The bottom surface of BC-60GP showed that GP fractions coated the BC fibers (Fig. 2k). The cross-section of BC–*Aloe* samples revealed that the 3D microstructure of BC was changed with the addition of each aloe portion. PF, GE and GP portions affected BC fiber synthesis, producing different internal microstructures (Fig. 2c, f, i and l). Compartmentalization of the 3D microstructure was mainly observed in BC-60PF samples (Fig. 2f). The specific changes observed in the 3D microstructure of the BC–*Aloe* samples in comparison with the BC samples had also been previously described in the literature (Tokoh et al. 2002a, b; Whitney et al. 1998). Furthermore, those authors suggested the presence of cell wall polysaccharides

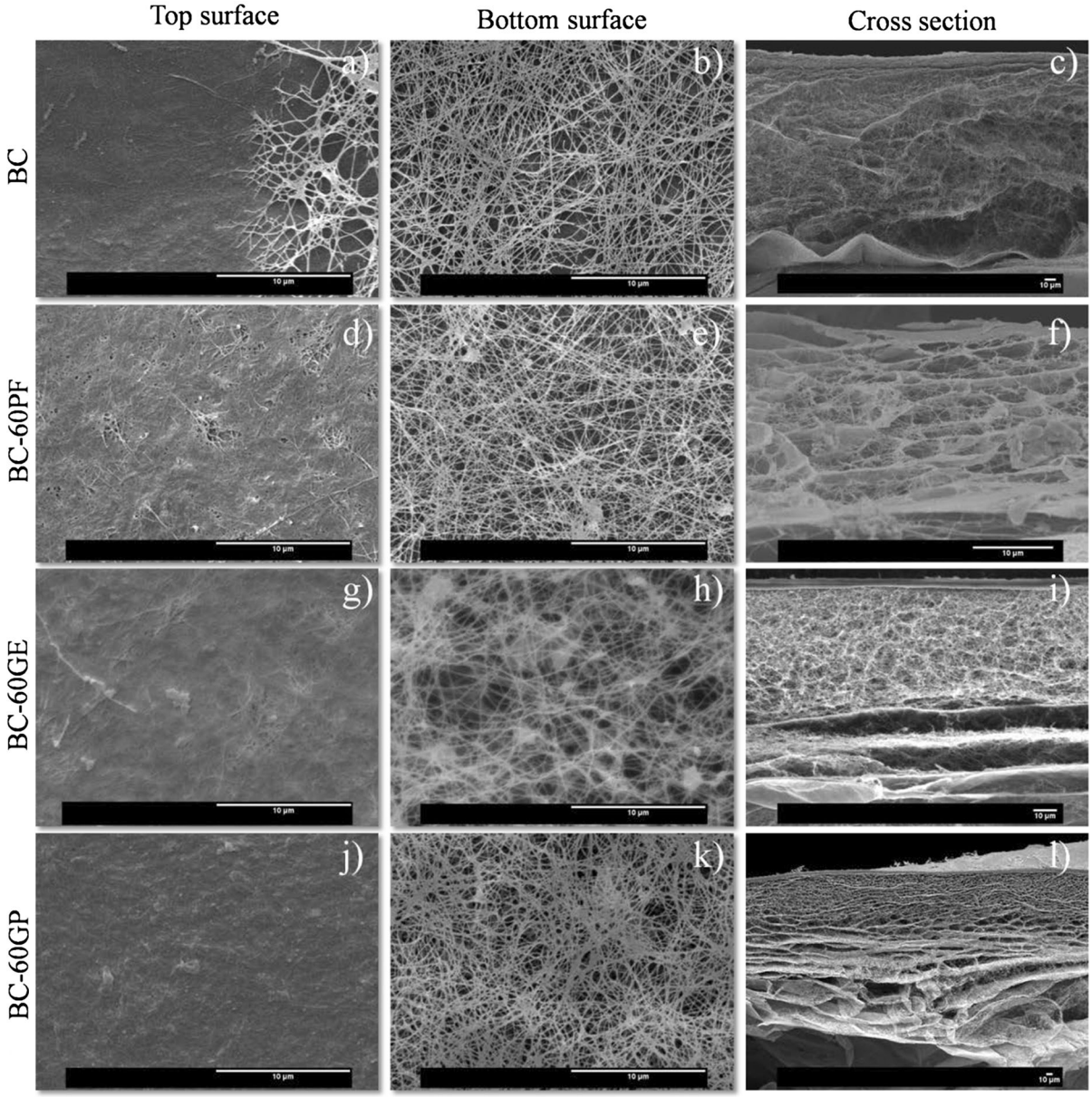

Fig. 2 SEM micrographs of freeze-dried BC–*Aloe* and BC samples. Entangled surface, porous surface and cross-section of BC (**a**–**c**), BC-60PF (**d**–**f**), BC-60GE (**g**–**i**) and BC-60GP (**j**–**l**) samples, subsequently. SEM micrographs were taken at ×5000 (**a**, **b**, **d**, **e**, **g**, **h**, **j** and **k**), ×430 (**c**), ×3000 (**f**), ×900 (**i**) and ×250 (**l**) magnification

during the BC synthesis, coating the fiber surface as a result of crosslinking between these polysaccharides and BC, collapsing the cellulose fibers and consequently increasing the fiber width (Tokoh et al. 2002a, b; Whitney et al. 1998). In this study, an increase of the average fiber width was observed from 87.4 ± 1.9 nm (BC) to 90.6 ± 2.1 nm (BC-60PF), 122.3 ± 3.4 nm (BC-60GE) and 128.9 ± 3.8 nm (BC-60GP). The bottom side has a higher porosity than the top (air-medium interface). Pure BC and PF and GE composites exhibit 40 % porosity, while the porosity of BC-60GP decreased slightly to 31 % after incorporation. The surface fiber density remained between three and four fibers/µm^2. The interactions between BC and the *Aloe* compounds led to pore occlusion and changes in the crystallinity and water uptake by the miscellaneous

surface chemical features produced by *Aloe* supplementation.

Figure 3 shows the X-ray diffraction patterns of the BC, BC-60PF, BC-60GE and BC60-GP samples. The three main peaks centered at 14.6°, 16.7° and 22.5° are attributed to the typical profile of a cellulose I polymorph (Nieduszy and Preston 1970). No significant shifts of the Bragg angle of the characteristics peaks were detected, but a decrease in the crystallinity and intensity of peaks was evident in BCAC, as shown in Table 1. The degree of crystallinity values followed this sequence: CB-60GP (35.8 %) < CB-60PF (43.5 %) < CB-60GE (44.8 %) < CB (51.9 %). This reduction was assigned to the insertion of amorphous phases, such as a polysaccharide fraction (PF), containing mannan or *Aloe vera* gel (GE, GP) into the BC during biosynthesis. However, the parameters of the BC unit cell remained unaltered. The insertion of the mannan groups has been reported to disturb the growth of BC crystallite, reducing the size by sticking to the surface of the newly formed microfibrils, blocking the ribbon formation (Tokoh et al. 1998). A smaller size of crystallite (3.9 nm) is observed in the presence of PF, followed by BC-60GP (4.4 nm), BC-60GE (4.8 nm) and BC (5.4 nm). Consequently, substantial changes in the mechanical properties of the membranes can be expected.

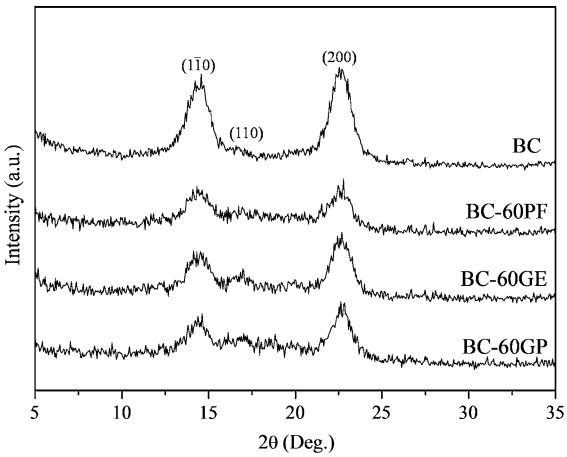

Fig. 3 X-ray diffractogram of BC and BC–*Aloe* scaffolds

Table 1 Crystallinity index and crystallite size of BC, BC-60PF, BC-60GE and BC-60GP

BC–*Aloe* scaffolds	χ_c (%)	Crystallite size (nm)
BC	51.9	5.4
BC-60PF	43.5	3.9
BC-60GE	44.8	4.8
BC-60GP	35.8	4.4

In order to investigate the integrity of membranes in hydrogel form, the samples were submitted to tensile strength tests. Summarized data are present in Table 2. The pure BC exhibits the highest Young's modulus (26.90 ± 2.18 kPa) and tensile strength (482.88 ± 35.42 kPa) and the lowest elongation at break (21.11 ± 0.72 %). The BC-60GP (72.89 ± 3.89 %) presented the highest elongation at break, followed by BC-60GE (70.36 ± 4.03 %) and BC-60PF (61.61 ± 3.92 %). The Young's modulus and tensile strength showed the same sequence: BC-60GE (3.71 ± 0.10 and 207.58 ± 8.92 kPa), BC-60GP (4.86 ± 0.64 and 238.39 ± 18.59 kPa) and BC-60PF (7.79 ± 0.32 and 262.72 ± 12.15 kPa), respectively. These alterations

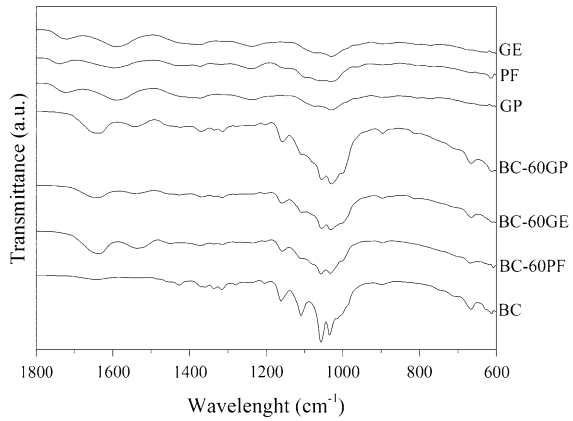

Fig. 4 FTIR spectra of F, G, T, BC and BC–*Aloe* scaffolds

Table 2 Mechanical properties of BC, BC-60PF, BC-60GE and BC-60GP

Mechanical property	BC	BC-60PF	BC-60GE	BC-60GP
E (kPa)	26.9 ± 2.2	7.8 ± 0.3	3.7 ± 0.1	4.9 ± 0.6
ε_b (%)	21.1 ± 0.7	61.6 ± 3.9	70.4 ± 4.0	72.9 ± 3.9
σ (MPa)	0.48 ± 0.03	0.26 ± 0.01	0.21 ± 0.09	0.24 ± 0.02

seem to be correlated with the increase of the amorphous phase in BC, which is deposited onto the surface of microfibrils, forming hotspots in some of the regions susceptible to breakage. Consequently, the number of intermolecular interactions (hydrogen bonds), which confers rigidity to the structure, is reduced. Furthermore, the presence of an amorphous phase between BC microfibrils allows the movement of fibers when pulling force is applied, thereby increasing the extensibility of the material. As the mechanical properties are closely linked to the microstructure and crystallinity of the material, the BC–*Aloe vera* composites presented a significant ($p < 0.05$) change in extensibility and elastic characteristics because of the high content of gel, expressed by increasing the elongation before breaking followed by decreasing the Young's modulus and tensile strength of the samples. Previous studies reported a decrease in the elasticity modulus and tensile strength up to 30 % of *Aloe* gel incorporation into BC or chitosan films (Saibuatong and Phisalaphong 2010; Khoshgozaran-Abras et al. 2012). Furthermore, the composites exhibited similar elasticity values to those evaluated for skin reported by Bader and Bowker (1983) and Pailler-Mattei et al. (2008). The elongation at break of the BC–*Aloe* composites is in the same range as those of excised human skin (dermis and

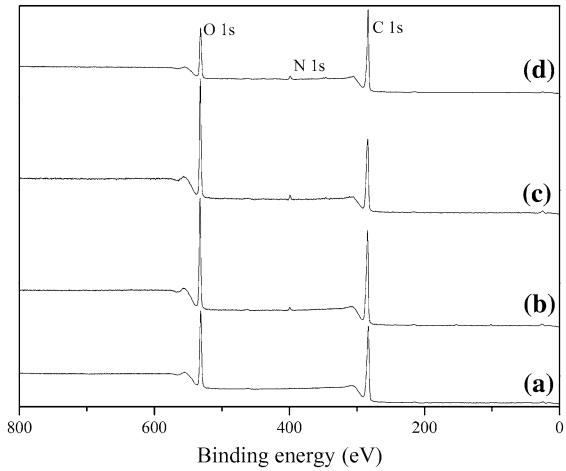

Fig. 5 XPS spectra *a* BC, *b* BC-60PF, *c* BC-60GE and *d* BC-60GP

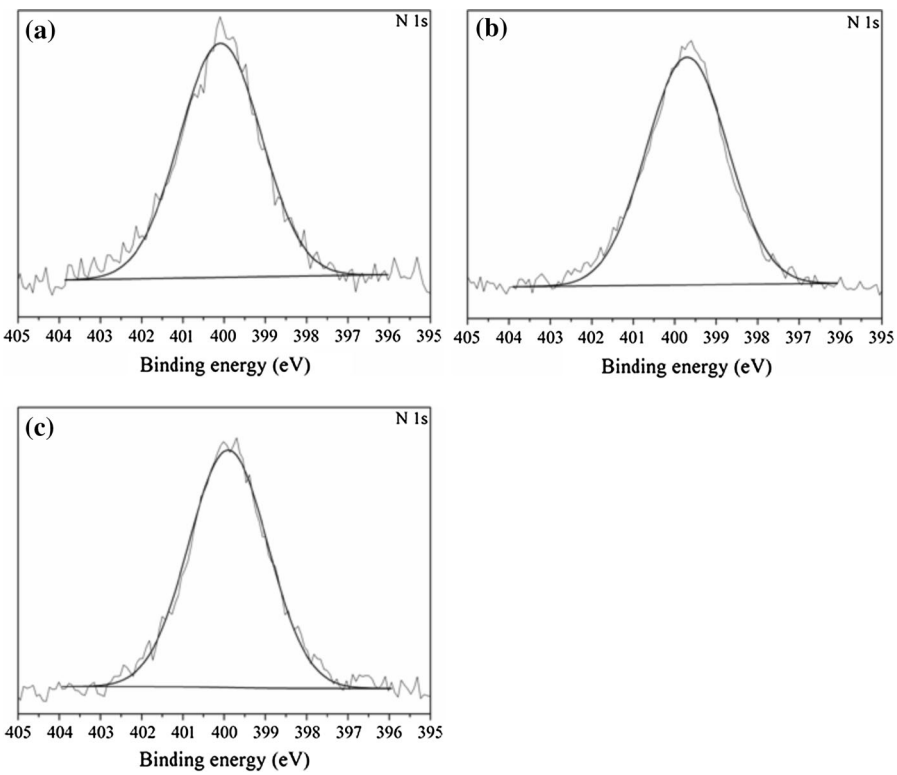

Fig. 6 Deconvolution of N1s peaks: **a** BC-60PF, **b** BC-60GE, and **c** BC-60GP

epidermis) determined by in vitro tests, but the tensile strength is one to two orders of magnitude lower (Ní Annaidh et al. 2012), which is expected since BC composites do not contain cells and connective tissue layers as in excised skin. These results indicate that the BC–*Aloe* composites could be applied in tissue engineering applications.

The FTIR spectra of PF, GE, GP and BC composites are shown in Fig. 4. The characteristic bands of BC at 3346 cm^{-1} stretching vibration (O–H), 2897 cm^{-1} stretching (C–H), 1427 cm^{-1} bending vibration in plane (HCH and OCH), 1161 cm^{-1} asymmetric vibrations (C–O–C) and 1109 cm^{-1} symmetric vibration (C–C) were present in all BC membranes (Kacurakova et al. 2002; Oh et al. 2005). In the high energy region, no significant difference between BC and BCAC was detected (data not shown), but in the low energy region an increase at 1648 cm^{-1} was observed and a shoulder appears at 1542 cm^{-1}. These bands are related to the presence of amide I and II (C=O and C–N stretch, N–H bending, respectively), probably because of an intramolecular interaction of this compound present in PF, GE and GP in BC (Saibuatong and Phisalaphong 2010). In addition, the presence of glucomannans and galactoglucomannans can be verified by the C–H ring vibration at 872 and 814 cm^{-1}. However, only the last band in BC-60GP and BC-60GE was detected, suggesting an incorporation of those polysaccharides into the membranes (Kacurakova et al. 2000).

The changes in the surface chemistry of BC, induced by medium supplementation with *Aloe* portions (BCAC), were analyzed using X-ray photoelectron spectroscopy (XPS). Figures 5, 6 and 7 show the spectra and decovoluted peaks of N1s and C1s for BC and BCAC, respectively. Data are summarized in Table 3.

The spectra (Fig. 5) show the presence of a nitrogen peak only for BCAC. The nitrogen peak around 400.0 eV (Fig. 6) in CB-60F and 60G CB–CB-60T reveals the presence of amines and amides in their respective structures, which are not present in pure BC (Tokoh et al. 1998). The most intense peak in the C1s region (Fig. 2a C2) is assigned to the C-O bonds from cellulose at 286.3 eV. A smaller contribution of C1 (284.5 eV) and C3 (288.1 eV) peaks is attributed to a single bond carbon–carbon (C–C) and a single bound carbon between two oxygen atoms (O–C–O),

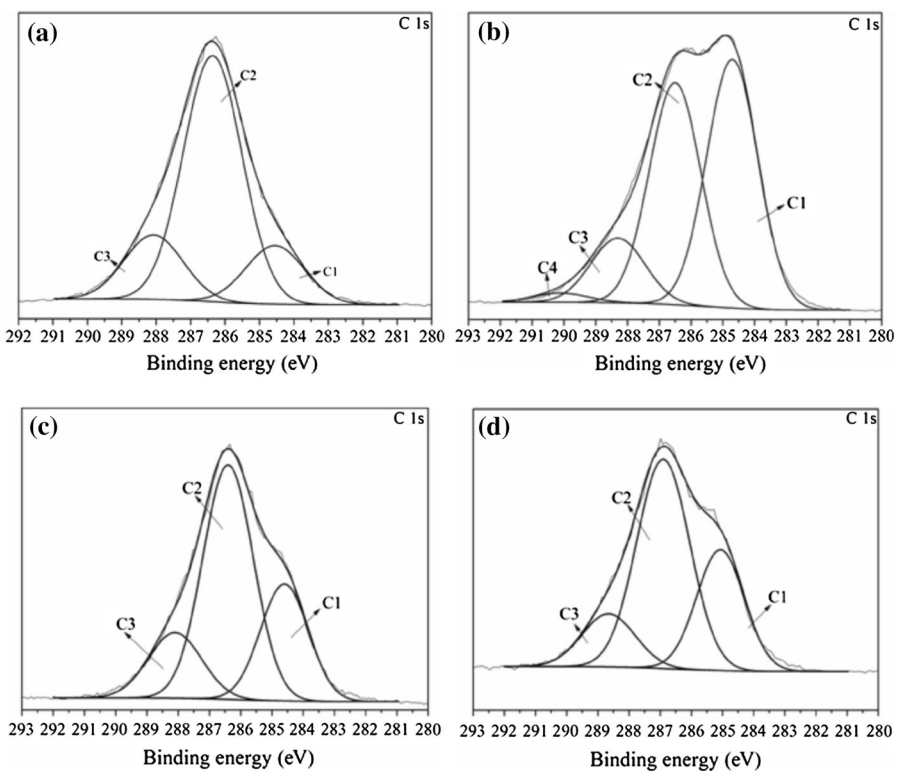

Fig. 7 Deconvolution of C1s peaks: **a** BC, **b** BC-60PF, **c** BC-60GE and **d** BC-60GP

Table 3 Assignments for the deconvolution of C1s, O1s and N1s for BCAC

Element	Binding energy (eV)				Assignment
	BC	BC-60PF	BC-60GE	BC-60GP	
C1	284.5	284.7	284.6	285.0	C–C/C–H[2,3]
C2	286.3	286.5	286.6	286.9	C–O/C–N[2,4]
C3	288.1	288.3	288.1	288.6	O–C–O/C=O[2,3]
C4		290.1			CO_3^5
N1		400.0	399.7	399.9	N from amines, amides or lactams[2]

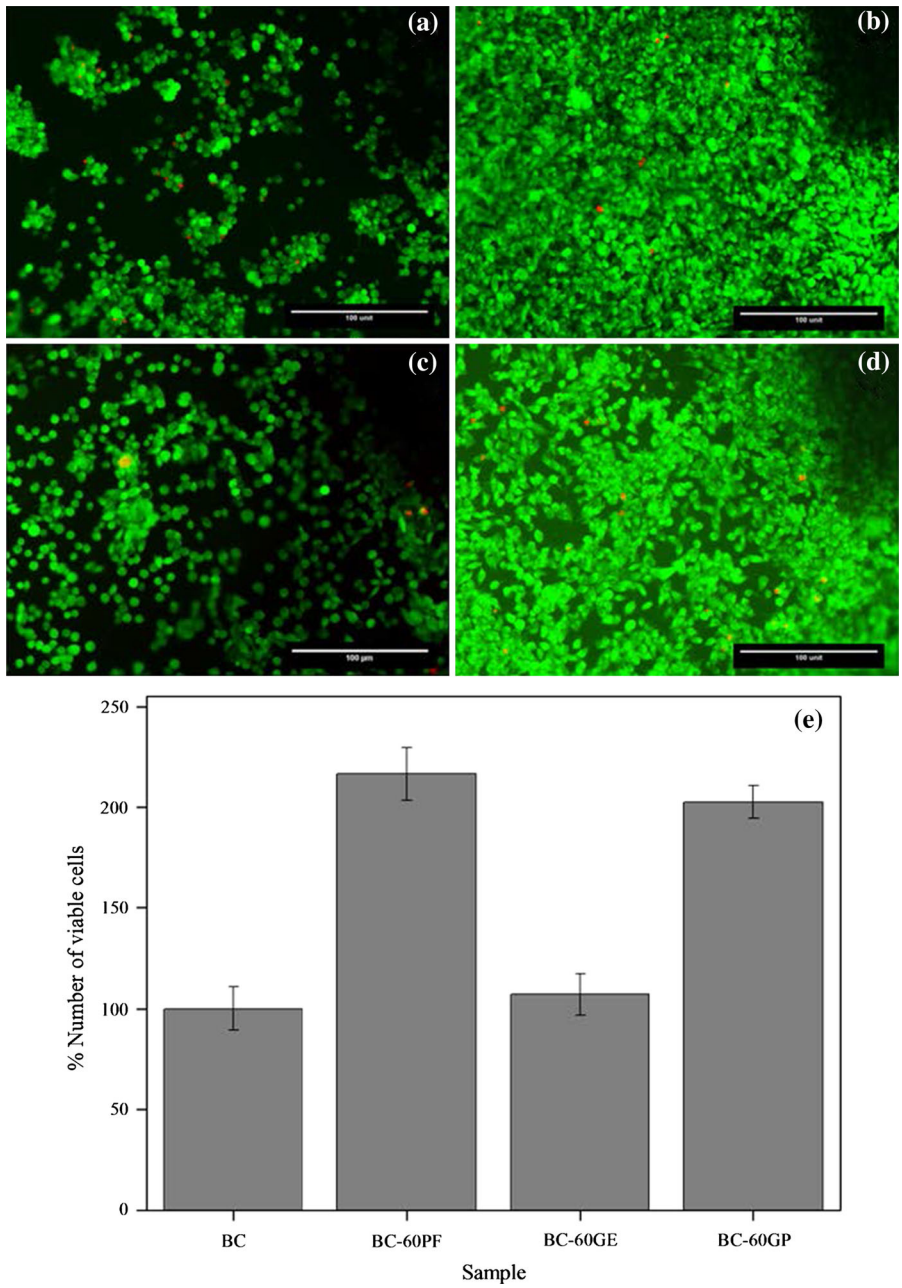

Fig. 8 L929 cells cultured for 48 h on the entangled surface of BC (**a**), BC-60PF (**b**), BC60GE (**c**) and BC-60GP (**d**); cell viability on different membranes (normalized with respect to pure BC) (**e**). L929 cells were stained with the Live/Dead® assay kit (*green* live cells and *red* dead cells). (Color figure online)

respectively (Cagniant et al. 2002). Since pure cellulose is composed of β-D-glucopyranose units and this structure consists of five carbons, in which four of them are bonded to one atom of oxygen and one carbon bonds two oxygen atoms, the presence of C2 and C3 peaks is expected. Then, the presence of a C1 peak suggests non-cellulosic compounds, which corresponds to unoxidized organic carbon in BC (Carlsson and Strom 1991). The C1, C2 and C3 peaks are present in BC-60PF (Fig. 2b; 284.5, 286.5 and 288.3 eV, respectively), BC-60GE (Fig. 2c; 284.6, 286.6 and 288.1 eV, respectively) and BC-60GP (Fig. 2d; 285.0, 286.9 and 288.6 eV, respectively). The BC-60PF presents a C4 peak at 290.1 eV assigned to the presence of carbonates (Yu et al. 2012). The increase of the C1 peak for BC-60PF, BC-60GE and BC-60GP confirms the insertion of aliphatic chains into these samples.

The viability of L929 cells cultured on entangled surfaces (top surface) of BC–*Aloe* and BC samples was analyzed by the Live/Dead® assay kit. Figure 8 shows that L929 cells remained viable (green) after 48 h of culture on BC–*Aloe* (b, c and d) and BC (a) samples. Qualitatively, viable cells fully covered the surface of BC-60PF (b) showing a strong adhesion between L929 cells and the scaffold surface. Similar results were also observed between the L929 cell culture on the BC-60GP (d) surface. L929 cells remained viable after 48 h of culture on the BC (a) and BC-60GE (c) surfaces; however, fewer cells adhered when compared with BC-60PF (b) and BC-60GP (d). Figure 8e shows the number of viable cells normalized with respect to pure BC. All samples sustained viable cells after 48 h, but the surface of BC-60PF exhibited higher levels of viable cells when compared to the other samples. Cell viability on the BC-60GE sample was similar to pure BC. As revealed by XPS, the BC–*Aloe* samples contain nitrogenous compounds in their structure. The presence of these nitrogenous compounds can be one of the factors that could improve adhesion between cells and BC–*Aloe* (Pertile et al. 2010; Silva et al. 2013a).

Conclusions

Bacterial nanocellulose and *Aloe vera* composites were synthesized in situ using mannitol-based medium supplemented with three different *Aloe vera* portions (*Aloe vera* gel pulp, *Aloe vera* gel extract and a polysaccharide fraction under static conditions). The incorporation of *Aloe vera* extract fractions during nanocellulose biosynthesis resulted in biocomposites with changes in the microstructure, chemical composition and mechanical properties compared to pure nanocellulose. Moreover, very similar skin mechanical properties were found in the hydrated state for both BC-60PF and BC-60GP samples. Cell viability assays revealed a strong adhesion between L929 cells and the surface of BC and BCAC. The results indicated that this material could be successfully applied as the scaffold material for several biomedical applications.

Acknowledgments The authors acknowledge the financial support of the Coordination of Improvement of Higher Education Personnel (CAPES, Brazil), Financier of Studies and Projects (FINEP, Brazil) and National Council for Scientific and Technological Development (CNPq, Brazil). The authors also appreciate the commitment and support of the UFSC laboratory teams: INTELAB, LAMATE, LFFS and LCME at UFSC.

References

Bader DL, Bowker P (1983) Mechanical characteristics of skin and underlying tissues in vivo. Biomaterials 4:305–308

Berti FV, Rambo CR, Dias PF, Porto LM (2013) Nanofiber density determines endothelial cell behavior on hydrogel matrix. Mater Sci Eng C 33:4684–4691

Cagniant D, Magri P, Gruber R, Berlozecki S, Salbut PD, Bimer J, Nansé G (2002) Ammoxidation of cellulose—a structural study. J Anal Appl Pyrol 65:1–23

Campestrini LH, Silveira JLM, Duarte MER, Koop HS, Noseda MD (2013) NMR and rheological study of Aloe barbadensis partially acetylated glucomannan. Carbohydr Polym 94:511–519

Carlsson CMG, Strom G (1991) Reduction and oxidation of cellulose surfaces by means of cold-plasma. Langmuir 7:2492–2497

Chang CY, Zhang LN (2011) Cellulose-based hydrogels: present status and application prospects. Carbohydr Polym 84:40–53

Czaja WK, Young DJ, Kawecki M, Brown RM (2007) The future prospects of microbial cellulose in biomedical applications. Biomacromolecules 8:1–12

Grace OM, Simmonds MSJ, Smith GF, van Wyk AE (2008) Therapeutic uses of *Aloe* L. (Asphodelaceae) in southern Africa. J Ethnopharmacol 119:604–614

Grindlay D, Reynolds T (1986) The aloe-vera phenomenon—a review of the properties and modern uses of the leaf parenchyma gel. J Ethnopharmacol 16:117–151

Guo J, Catchmark JM (2012) Surface area and porosity of acid hydrolyzed cellulose nanowhiskers and cellulose produced by Gluconacetobacter xylinus. Carbohydr Polym 87:1026–1037

Jithendra P, Rajam AM, Kalaivani T, Mandal AB, Rose C (2013) Preparation and characterization of *Aloe vera*

blended collagen–chitosan composite scaffold for tissue engineering applications. ACS Appl Mater Interfaces 14:7291–7298

Kacurakova M, Capek P, Sasinkova V, Wellner N, Ebringerova A (2000) FT-IR study of plant cell wall model compounds: pectic polysaccharides and hemicelluloses. Carbohydr Polym 43:195–203

Kacurakova M, Smith AC, Gidley MJ, Wilson RH (2002) Molecular interactions in bacterial cellulose composites studied by 1D FT-IR and dynamic 2D FT-IR spectroscopy. Carbohydr Res 337:1145–1153

Khoshgozaran-Abras S, Azizi MH, Hamidy Z, Bagheripoor-Fallah N (2012) Mechanical, physicochemical and color properties of chitosan based-films as a function of *Aloe vera* gel incorporation. Carbohydr Polym 87:2058–2062

Kim K, Kim H, Kwon J, Lee S, Kong H, Im SA, Lee YH, Lee YR, Oh ST, Jo TH, Park YI, Lee CK, Kim K (2009) Hypoglycemic and hypolipidemic effects of processed *Aloe vera* gel in a mouse model of non-insulin-dependent diabetes mellitus. Phytomedicine 16:856–863

Klemm D, Heublein B, Fink HP, Bohn A (2005) Cellulose: fascinating biopolymer and sustainable raw material. Angew Chem Int Edit 44:3358–3393

Müller D, Mandelli JS, Marins JA, Soares BG, Porto LM, Rambo CR, Barra GMO (2012) Electrically conducting nanocomposites: preparation and properties of polyaniline (PAni)-coated bacterial cellulose nanofibers (BC). Cellulose 19:1645–1654

Ní Annaidh A, Bruyère K, Destrade M, Gilchrist MD, Otténio M (2012) Characterization of the anisotropic mechanical properties of excised human skin. J Mech Behav Biomed Mater 5:139–148

Nieduszy I, Preston RD (1970) Crystallite size in natural cellulose. Nature 225:273–275

Oh SY, Yoo DI, Shin Y, Seo G (2005) FTIR analysis of cellulose treated with sodium hydroxide and carbon dioxide. Carbohydr Res 340:417–428

Pailler-Mattei C, Bec S, Zahouani H (2008) In vivo measurements of the elastic mechanical properties of human skin by indentation tests. Med Eng Phys 30:599–606

Pereira R, Carvalho A, Vaz DC, Gil MH, Mendes A, Bártolo P (2010) Development of novel alginate based hydrogel films for wound healing applications. Int J Biol Macromol 52:221–230

Pereira R, Mendes A, Bártolo P (2013) Alginate/*Aloe vera* hydrogel films for biomedical applications. Procedia CIRP 5:210–215

Pertile RAN, Andrade FK, Alves C Jr, Gamna M (2010) Surface modification of bacterial cellulose by nitrogen-containing plasma for improved interaction with cells. Carbohyd Polym 82:692–698

Reynolds T (2004) Aloes: the genus *Aloe*. CRC Press, London

Saibuatong OA, Phisalaphong M (2010) Novo *Aloe vera*-bacterial cellulose composite film from biosynthesis. Carbohydr Polym 79:455–460

Shaik J, Mohammed JS, McShane MJ, Mills DK (2013) Behavior of articular chondrocytes on nanoengineered surfaces Nano LIFE 3:1–23

Silva SS, Caridade SG, Mano JF, Reis RL (2013a) Effect of crosslinking in chitosan/*Aloe vera*-based membranes for biomedical applications. Carbohydr Polym 98:581–588

Silva SS, Popa EG, Gomes ME, Cerqueira M, Marques AP, Caridade SG, Teixeira P, Sousa C, Mano JF, Reis LR (2013b) An investigation of the potential application of chitosan/aloe-based membranes for regenerative medicine. Acta Biomater 9:6790–6797

Stumpf TR, Pértile RAN, Rambo CR, Porto LM (2013) Enriched glucose and dextrin mannitol-based media modulates fibroblast behavior on bacterial cellulose membranes. Mater Sci Eng C 33:4739–4745

Tang WH, Jia SR, Jia YY, Yang HJ (2010) The influence of fermentation conditions and post-treatment methods on porosity of bacterial cellulose membrane. World J Microbiol Biotechnol 26:125–131

Tokoh C, Takabe K, Fujita M, Saiki H (1998) Cellulose synthesized by Acetobacter xylinum in the presence of acetyl glucomannan. Cellulose 5:249–261

Tokoh C, Takabe K, Sugiyama J, Fujita M (2002a) Cellulose synthesized by Acetobacter xylinum in the presence of plant cell wall polysaccharides. Cellulose 9:65–74

Tokoh C, Takabe K, Sugiyama J, Fujita M (2002b) CP/MAS (13)C NMR and electron diffraction study of bacterial cellulose structure affected by cell wall polysaccharides. Cellulose 9:351–360

Watanabe K, Tabuchi M, Morinaga Y, Yoshinaga F (1998) Structural features and properties of bacterial cellulose produced in agitated culture. Cellulose 5:187–200

Whitney SEC, Brigham JE, Darke AH, Reid JSG, Gidley MJ (1998) Structural aspects of the interaction of mannan-based polysaccharides with bacterial cellulose. Carbohydr Res 307:299–309

Yu L, Falco C, Weber J, White RJ, Howe JY, Titirici M-M (2012) Carbohydrate-derived hydrothermal carbons: a thorough characterization study. Langmuir 28:12373–12383

Zhang LN, Tizard IR (1996) Activation of a mouse macrophage cell line by acemannan: the major carbohydrate fraction from *Aloe vera* gel. Immunopharmacology 35:119–128